Published online 4 July 2016

Nucleic Acids Research, 2016, Vol. 44, No. 20 ***9891–9901***
doi: 10.1093/nar/gkw605

The functional requirement of two structural domains within telomerase RNA emerged early in eukaryotes

Joshua D. Podlevsky, Yang Li and Julian J.-L. Chen*

School of Molecular Sciences, Arizona State University, Tempe, AZ 85287, USA

Received May 04, 2016; Revised June 22, 2016; Accepted June 23, 2016

ABSTRACT

Telomerase emerged during evolution as a prominent solution to the eukaryotic linear chromosome end-replication problem. Telomerase minimally comprises the catalytic telomerase reverse transcriptase (TERT) and telomerase RNA (TR) that provides the template for telomeric DNA synthesis. While the TERT protein is well-conserved across taxa, TR is highly divergent amongst distinct groups of species. Herein, we have identified the essential functional domains of TR from the basal eukaryotic species *Trypanosoma brucei*, revealing the ancestry of TR comprising two distinct structural core domains that can assemble *in trans* with TERT and reconstitute active telomerase enzyme *in vitro*. The upstream essential domain of *T. brucei* TR, termed the template core, constitutes three short helices in addition to the 11-nt template. Interestingly, the trypanosome template core domain lacks the ubiquitous pseudoknot found in all known TRs, suggesting later evolution of this critical structural element. The template-distal domain is a short stem-loop, termed equivalent CR4/5 (eCR4/5). While functionally similar to vertebrate and fungal CR4/5, trypanosome eCR4/5 is structurally distinctive, lacking the essential P6.1 stem-loop. Our functional study of trypanosome TR core domains suggests that the functional requirement of two discrete structural domains is a common feature of TRs and emerged early in telomerase evolution.

INTRODUCTION

The emergence of linear chromosomes during the early evolution of eukaryotes prompted the need for special mechanisms to protect chromosome ends and prevent DNA shortening, a consequence of the end-replication problem (1). Telomeres are specialized DNA-protein structures that cap chromosome ends and safeguard against genome instability (2). Telomere function is highly dependent on telomeric DNA length, which is maintained by the telomerase ribonucleoprotein (RNP) enzyme that is specialized for telomeric DNA synthesis (3,4). The functional core of the telomerase RNP comprises the catalytic telomerase reverse transcriptase (TERT) and integral telomerase RNA (TR) component that harbors the template sequence for DNA synthesis (5). TRs are remarkably divergent in size, sequence and secondary structure (6). This massive disparity was presumably driven by TR adopting a variety of structural elements for binding species-specific proteins in different evolutionary lineages for employing a multitude of diverse biogenesis pathways.

Despite the extensive disparities amongst TRs from distinct groups of species in eukaryotes, there has been considerable progress toward the identification of common, essential and implied ancestral TR structural elements. Secondary structure determination of TRs from vertebrates, invertebrates, fungi and ciliates revealed two critical and conserved structural features: (i) a template-proximal pseudoknot and (ii) a template-distal stem-loop moiety (7–10). While the precise functions of these elements have yet to be determined, the pseudoknot structure has been proposed to facilitate template positioning within the TERT active site (11). The vertebrate TR template-distal stem-loop moiety, termed conserved regions 4 and 5 (CR4/5), comprises a helical three-way-junction with two short highly conserved stem-loops, P6 and P6.1, and is absolutely critical for telomerase enzymatic function (12). Vertebrate CR4/5 has been postulated to allosterically facilitate TERT domain folding based on its binding affinity and close proximity to two TERT domains (13,14). In the invertebrate echinoderm TR, a template-distal helical region that lacks a three-way-junction can reconstitute telomerase activity *in trans*, which is functionally equivalent to vertebrate CR4/5 and thus termed equivalent CR4/5 (eCR4/5) (10). In contrast, budding yeast template-distal moieties are structurally similar to vertebrate CR4/5, comprising a three-way-junction of large helices which, however, lack the short P6.1 stem-loop (15). Interestingly, the recent identification and functional characterization of filamentous fungal TRs reconciled the disparity amongst budding yeast and vertebrate TR template-distal stem-loop moieties (8). Filamentous fungal and fission yeast TRs contain template-distal moieties with secondary structures virtually identical to verte-

*To whom correspondence should be addressed. Tel: +1 480 965 3650; Fax: +1 480 965 2747; Email: jlchen@asu.edu

brate CR4/5 and are absolutely essential for telomerase enzymatic activity (8,14). The immense structural and functional conservation in both vertebrate and fungal TRs indicate that CR4/5 is an ancestral TR structural element common to metazoan and fungal TRs.

Despite being the first identified, ciliate TRs are highly atypical compared to metazoan and fungal TRs (16). Ciliate TRs are transcribed by RNA polymerase (pol) III and contain a terminal poly(U) tract that is common for small RNAs (17), while vertebrate and fungal TRs are transcribed by RNA pol II with nascent poly(A) tails that are removed by 3′-end processing with the exception of budding yeast RNA pol II transcription termination by the Nrd1-Nab3-Sen1 pathway (18–24). The recently identified TR from the flagellated protozoan *Trypanosoma brucei* was found to be approximately one kilobase-pair in length, transcribed by RNA pol II, and the nascent transcript *trans* spliced with a spliced leader RNA common for trypanosome mRNAs (25,26). Additionally, *T. brucei* TR (*tbr*TR) contains canonical snoRNA box C/D moieties and is bound by the box C/D snoRNP proteins Nop58 and Snu13 (26). Flagellated protozoans are considered amongst the earliest branching eukaryotes (27,28), strongly supporting the prevalent RNA pol II machinery for TR transcription as ancestral and RNA pol III employed uniquely for ciliate TRs as later evolved. Discerning features common to all TRs has remained daunting. However, trypanosome TR is a plausible candidate for resolving the disparities amongst ciliate and vertebrate-fungal TRs to better expose the origins of telomerase RNP.

Herein, we report the functional and structural analyses of flagellate TR, revealing the minimal regions of the RNA necessary for *in vitro* reconstitution of trypanosome telomerase activity with the TERT protein. While the vast majority of flagellate TR is dispensable for telomerase activity, therein lies two conserved structural domains that can independently assemble with the TERT protein and are both required for telomerase enzymatic function. The trypanosome TR structure brings to light critical features of the earliest TRs within eukaryotes, revealing that the functional requirement of two TR domains for telomerase enzymatic function is an ancestral attribute of the unique telomerase enzyme.

MATERIALS AND METHODS

Cloning of TERT and TR genes

The *tbr*TERT and *tbr*TR genes were directly PCR amplified from genomic DNA (a generous gift from Dr. Juan Alfonzo) and cloned into pCITE-4a (Promega) and TOPO (Invtrogen) vectors, respectively. The *tbr*TERT gene was appended with an N-terminal FLAG tag to generate pNFLAG-*tbr*TERT.

Reconstitution of telomerase enzyme

Recombinant *tbr*TERT protein was synthesized from pNFLAG-*tbr*TERT in a 5 μl reaction of TnT Quick-coupled transcription/translation kit (Promega) at 30°C for 1 h, following the manufacturer's instructions. Various *tbr*TR RNA fragments were *in vitro* transcribed, gel purified and added at a final concentration of 1 μM to assemble with *tbr*TERT in RRL at 30°C for 30 min.

Telomerase activity assay

Telomerase activity was measured by the direct primer-extension activity assay (29). A 10 μl reaction was performed with 2 μl *in vitro* reconstituted *T. brucei* telomerase in 1x telomerase reaction buffer (50 mM Tris-HCl, pH 8.3, 2 mM DTT, 0.5 mM $MgCl_2$, 1 mM spermidine), 100 μM dTTP, 100 μM dATP, 5 μM dGTP, 0.165 μM α-^{32}P-dGTP (3000 Ci/mmol, 10 mCi/ml, Perkin-Elmer) and 1 μM $(TTAGGG)_3$ DNA primer. The reaction was incubated at 30°C for 1 h and terminated by phenol/chloroform extraction followed by ethanol precipitation. The telomerase extended products were electrophoresed on a 10% polyacrylamide/8 M urea denaturing gel, and the dried gel was exposed to a phosphorstorage screen and analyzed with a Molecular Imager FX-Pro (Bio-Rad). Total activity was normalized to the loading control and the relative activity was determined by normalizing the total activity to that of the reaction with the longest or the wild-type *tbr*TR fragments.

SHAPE analysis

The minimal *tbr*TR 5′- or 3′-fragments were PCR amplified with primers to append the 5′- and 3′-ends with SHAPE-specific adapter sequences, as previously described (30). These PCR products were used as templates for *in vitro* transcription, gel purified, and ethanol precipitated. Two picomoles of each purified minimal *tbr*TR fragment with SHAPE adapters was denatured in 0.5X TE buffer (pH 8.0) at 95°C for 2 min and immediately placed on ice for 2 min. The RNA was supplemented with a final concentration 1x RNA folding mix (100 mM HEPES, pH 8.0, 6 mM $MgCl_2$ and 100 mM NaCl), incubated at 30°C for 20 min, and divided in half. The RNA was treated with either 6.5 mM *N*-methylisatoic anhydride (NMIA) (Sigma) in anhydrous DMSO or DMSO alone, incubated at 30°C for 1 h and 25 min (five NMIA hydrolysis half-lives), and ethanol precipitated. One picomole of ^{32}P end-labeled primer was added to the RNA samples in 0.5X TE buffer, pH 8.0 and incubated at 65°C for 5 min, 35°C for 5 min, and then placed on ice. The mixture was supplemented with 1X SuperScript III First-strand buffer (50 mM Tris-HCl, pH 8.3, 75 mM KCl and 3 mM $MgCl_2$), 5 mM DTT, 0.5 mM each dNTP and 0.75 mM ddGTP or ddATP for the untreated RNA, followed by incubation at 52°C for 1 min, addition of 100 U SuperScript III RT (Life Technologies), and incubation at 52°C for 10 min. Alkaline hydrolysis was performed with a final concentration of 200 mM sodium hydroxide with incubation at 95°C for 5 min and stopped by the addition of Acid Stop solution (77 mM unbuffered Tris-HCl, 32% formamide and 8 mM EDTA) with incubation at 95°C for 5 min. The DNA products were resolved on a 6.8% polyacrylamide/8M urea denaturing gel. The gel was dried, exposed to a phosphorstorage screen, and imaged on a phosphorimager FX-Pro (Bio-Rad). Absolute reactivity was determined following the criteria described previously

(30). Briefly, NMIA reactivity was normalized by subtracting the lowest intensity value from all positions, followed by subtracting the intensity values of the DMSO control from the corresponding NMIA reaction.

Sequence alignment analysis

Corresponding genomic regions to the *tbr*TR (26) were excised from *T. congolense* (GenBank CAEQ01001861), *T. vivax* (HE573027) and *T. cruzi* (CH473328) genome data. The 5′- and 3′-ends of the other Trypanosome TRs sequences were defined by the helix forming the box C/D at the termini. Multiple alignment of these four Trypanosome TRs was performed within the program BioEdit using the ClustalW algorithm for the first-pass of the alignment. The alignments were further refined manually with highly conserved regions and known motifs as anchor points and covariation of predicted helices supported by SHAPE analysis. Co-variations were limited to Watson–Crick base-pairs and G:U pairings were treated as neutral variations.

Identification of *Trypanosoma grayi* TR

Each strand of the draft genome of *Trypanosoma grayi* (31) was analyzed with a search pattern generated in the Fragrep2 program (32) from the multiple sequence alignment of the four Trypanosome TRs annotated for regions of high conservation. The single hit for the *T. grayi* TR sequence was obtained from the *T. grayi* genome database and added to the Trypanosome TR multiple sequence alignment.

RESULTS

In vitro reconstitution of functional *T. brucei* telomerase

To discern the functional core within TR from early diverging flagellates, we reconstituted *T. brucei* telomerase enzyme by assembling *in vitro* synthesized *tbr*TR and *tbr*TERT in rabbit reticulocyte lysate (see Materials and Methods). Three *tbr*TR variants have been previously reported with distinct sizes of 892, 1358 and 1506 nt (Figure 1A), transcribed from a single locus with separate initiation and termination sites (25,26). All three *tbr*TR variants harbor the 11-nt template sequence for the synthesis of exact 5′-TTAGGG-3′ telomeric DNA repeats (Figure 1A). We investigated whether these *tbr*TR variants assemble with the *tbr*TERT protein and reconstitute telomerase activity *in vitro*. A primer extension assay of telomerase enzymes reconstituted with the three individual TR variants, *tbr*TR-v1, -v2 and -v3, using the DNA primer 5′-$(TTAGGG)_3$-3′ showed similar levels of activity with the characteristic 6-nt ladder banding pattern (Figure 1B, lanes 2–4). Thus, the larger *tbr*TR-v2 and -v3 variants do not appear to contain any additional elements necessary for telomerase activity *in vitro* and the shorter *tbr*TR-v1 variant is sufficient to associate with the TERT protein and reconstitute a full-level of activity.

The reconstituted *T. brucei* telomerase activity was dependent on the presence of *tbr*TR and *tbr*TERT (Figure 1C, lanes 2–4). As expected, the reconstituted activity was sensitive to high-temperatures or RNase A-treatment (Figure 1C, lanes 5 and 6) that are typical features of a telomerase

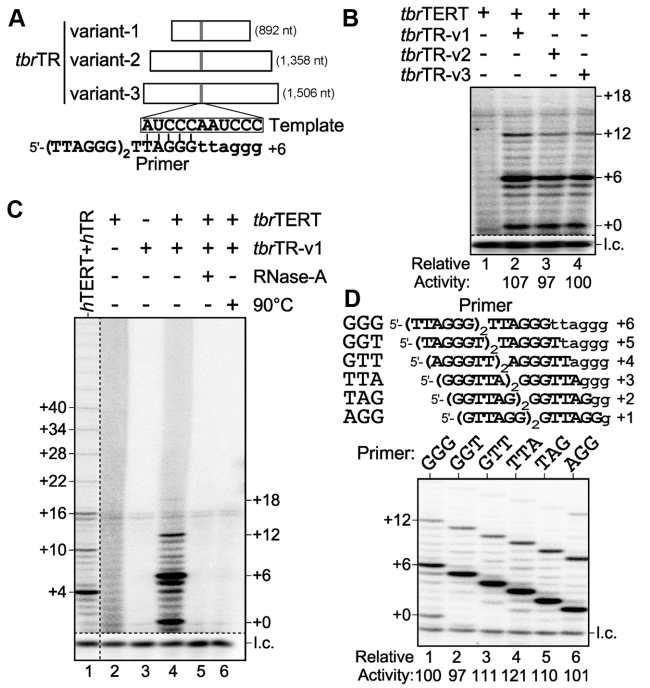

Figure 1. *In vitro* reconstitution of *T. brucei* telomerase. (**A**) Schematic of *tbr*TR variants. The sequence of the 11 nt template is annealed to an 18-mer telomeric DNA primer with the expected primer-extended product depicted (lowercase). The length of the three *tbr*TR variants -v1, -v2 and -v3 is denoted. (**B–D**) Activity assay of *in vitro* reconstituted *T. brucei* telomerase. (**B**) Direct primer-extension assay of *T. brucei* telomerase reconstituted from the three T7 transcribed *tbr*TR variants and synthetic *tbr*TERT. A *tbr*TERT-alone control reaction was included. (**C**) *T. brucei* telomerase functions as an RNP, requiring *tbr*TERT and *tbr*TR. Telomerases reconstituted with *tbr*TR-alone, *tbr*TERT-alone, treated with RNase A or 90°C heat denaturation were analyzed to control for the specific activity of the *T. brucei* telomerase RNP enzyme. Human telomerase reconstituted *in vitro* with hTR and hTERT was included for comparison of ladder-banding patterns. (**D**) Activity analysis of *T. brucei* telomerase using permuted DNA primers. The permuted sequences of the telomeric DNA primers are denoted with the expected primer-extended products depicted (lowercase). The +0 product resulted from the nucleolytic activity of *T. brucei* telomerase is only apparent with the 5′-$(TTAGGG)_3$-3′ primer. A ^{32}P-end-labeled 18-mer DNA primer was added prior to product purification as a loading control (l.c.) for DNA product recovery and loading. The number of nucleotides added to the primer are denoted beside the gel and the relative activity shown below the gel.

RNP enzyme. The faint background bands in the TERT-alone control reaction was likely from TERT using non-specific RNAs in the RRL as template (Figure 1C, lane 2), as this background activity was completely eliminated with the inclusion of RNase-A (Figure 1C, lane 5). The 6-nt ladder banding pattern of products generated by the reconstituted *T. brucei* telomerase was two nucleotides offset from human telomerase (Figure 1C, lanes 1 and 4), consistent with the two nucleotide permutation of the *tbr*TR template sequence, 3′-AUCCCAAUCCC-5′, compared with the human TR (hTR) template sequence, 3′-CAAUCCCAAUC-5′. When assayed using telomeric DNA primers with the six permutated sequences, *T. brucei* telomerase generated similar levels of activity with the expected offset banding patterns (Figure 1D), indicating correct primer-template alignment and specific template usage. Interestingly, a +0 prod-

uct was generated exclusively with the 5′-(TTAGGG)$_3$-3′ primer, presumably through the removal of the 3′-terminal dG by intrinsic nucleolytic activity of *T. brucei* telomerase followed by the incorporation of an α-^{32}P-dGTP residue (Figure 1D, lane 1). Similar nucleolytic activity has been reported for human and ciliate telomerases (33,34) Together, these data demonstrate the first *in vitro* reconstitution system for telomerase from *T. brucei*, an early diverging flagellate.

T. brucei TR contains two structural domains required for enzymatic activity

To identify regions within *tbr*TR necessary and sufficient for reconstituting telomerase activity, we carried out serial truncation analysis of the 892 nt *tbr*TR-v1 by shortening the RNA from either the 5′- or 3′-terminus (Figure 2A, top). Five truncated *tbr*TR fragments, termed A to E, were generated at ∼150 nt intervals with each fragment retaining the essential template sequence. These *tbr*TR truncated fragments were assembled with the *tbr*TERT protein in RRL and assayed for telomerase activity by direct primer-extension using the primer 5′-(TTAGGG)$_3$-3′ (Figure 2A, bottom). Fragments A, B and C with 3′-end serial truncations had severe defects for reconstituting telomerase activity, retaining merely 30–40% of full activity (Figure 2A, bottom, lanes 1–4). This result suggests that an element within *tbr*TR near the 3′-terminus is critical for telomerase activity. Fragment D, with the first 150 nt deleted, assembled efficiently with *tbr*TERT and generated an elevated level of activity compared with *tbr*TR-v1 (Figure 2A, bottom, lanes 1 and 5), indicating that the first 150 nt are dispensable for telomerase activity. The increased activity accompanying the 5′ truncation in fragment D potentially resulted from improved RNA folding of this RNA fragment *in vitro*. In contrast, fragment E, with the first 291 nt deleted, failed to reconstitute any detectable activity (Figure 2A, bottom, lane 6). Thus, the region between residues 151 and 291 of *tbr*TR-v1 contains an element(s) crucial for telomerase activity.

Vertebrate and fungal TRs comprise two separate structural domains, a template-proximal core and a template-distal element (8), that bind independently to TERT and are absolutely essential for telomerase enzymatic function. To determine whether *tbr*TR constitutes two distinct structural domains that can reconstitute telomerase activity *in trans*, we separated the minimal *tbr*TR fragment D into two shorter RNA fragments, the 5′ fragment 5F1 that contained residues 151 to 700 and the 3′ fragment 3F1 that contained residues 701 to 892 (Figure 2B, top). Interestingly, *T. brucei* telomerase reconstituted from the two physically separate RNA fragments 5F1 and 3F1 generated a level of activity similar to the single fragment D (Figure 2B, bottom, lanes 1–2). This result indicates that the two *tbr*TR fragments can reconstitute full activity *in trans*. Functional analysis of additional 5′ and 3′ truncated fragments in different combinations identified a functionally dispensable region spanning residues 501 to 700, as fragments 5F3 (residues 151 to 500) together with 3F1 (residues 701 to 892) reconstituted full activity (Figure 2B, lane 5). Unexpectedly, the larger fragment 5F2 (residues 151–600) together with fragment 3F1 reconstituted merely 58% of full activity (Figure 2B, lane 3) that may have resulted from suboptimal folding of the 5F2 fragment compared to the shorter 5F3 fragment. As a control, the largest 5′ and 3′ fragments, 5F1 and 3F3, were assayed individually. Consistent with our previous results with fragments A through C (Figure 2A), the fragment 5F1 alone reconstituted ∼30–40% activity compared to fragment D (Figure 2B, lane 6), while fragment 3F3 that lacked the template sequence did not generate any discernible activity (Figure 2B, lane 7). This result demonstrates that *tbr*TR contains two discrete structural domains that independently associate with the TERT protein *in trans*, a feature commonly conserved across vertebrate and fungal TRs.

To further map the essential regions within the minimal 5′ fragment 5F3, we introduced truncations at ∼50 or 15 nt intervals from either the 5′- or 3′-termini (Figure 3A, top). These serially truncated 5F3 fragments, -a to -g, were assembled *in trans* with fragment 3F1 and the *tbr*TERT protein, then assayed for telomerase activity. The activity assay revealed fragment 5F3-g (248–449 nt) as the minimal 5F3 fragment for generating functional *T. brucei* telomerase (Figure 3A, bottom, lane 9). Additional 5′- or 3′-deletions of the 5F3 fragment within the region spanning residues 248–449 severely impaired activity (Figure 3A, bottom, lanes 3, 7 and 8). Interestingly, the 5F3-g fragment generated significantly greater activity than the parental 5F3 fragment, conceivably by removing regions that were poorly folded or otherwise interfered with proper assembly of the RNA with the TERT protein (Figure 3A, bottom, lane 9).

Our truncation analysis of *tbr*TR successfully identified two minimal regions that are sufficient for telomerase enzymatic function: the template-containing region, residues 248–449 of fragment 5F3-g and the template-distal region, residues 701–892 of fragment 3F1. To determine whether these two regions fold into stable secondary structures similar to the pseudoknot and CR4/5 domains that are conserved throughout vertebrate and fungal TRs, we performed computational analysis of these sequences using the mFold program (35) to predict possible secondary structures. For the template-containing fragment 5F3-g, the template sequence was constrained as single-stranded and the template-flanking sequences were predicted to form three helical regions, termed Helix-I, -II and -III (Figure 3B, top). The template-distal fragment 3F1 was predicted to form a singular, extended stem-loop structure (Figure 3C, top).

We then performed structure-based truncation analyses on fragments 5F3-g and 3F1 to further minimize these two essential regions. We first introduced helical truncations into fragment 5F3-g to increasingly remove portions of the putative Helix-I, generating H1-Δ1, -Δ2 and -Δ3 (Figure 3B, top). The H1-Δ1 and -Δ2 RNA fragments, together with the 3F1 fragment and *tbr*TERT, reconstituted significant telomerase activity at 64% and 95% of the parental fragment 5F3-g, respectively, (Figure 3B, bottom, lanes 1–3). In contrast, the H1-Δ3 fragment—with most of Helix-I removed—failed to generate any detectable activity (Figure 3B, bottom, lane 4). Additional truncations or mutations introduced to the *tbr*TR H1-Δ2 RNA fragment abolished telomerase activity (Supplementary Figure S1). This suggests that the *tbr*TR H1-Δ2 RNA fragment contains the minimal region of the putative Helix-I essential for telom-

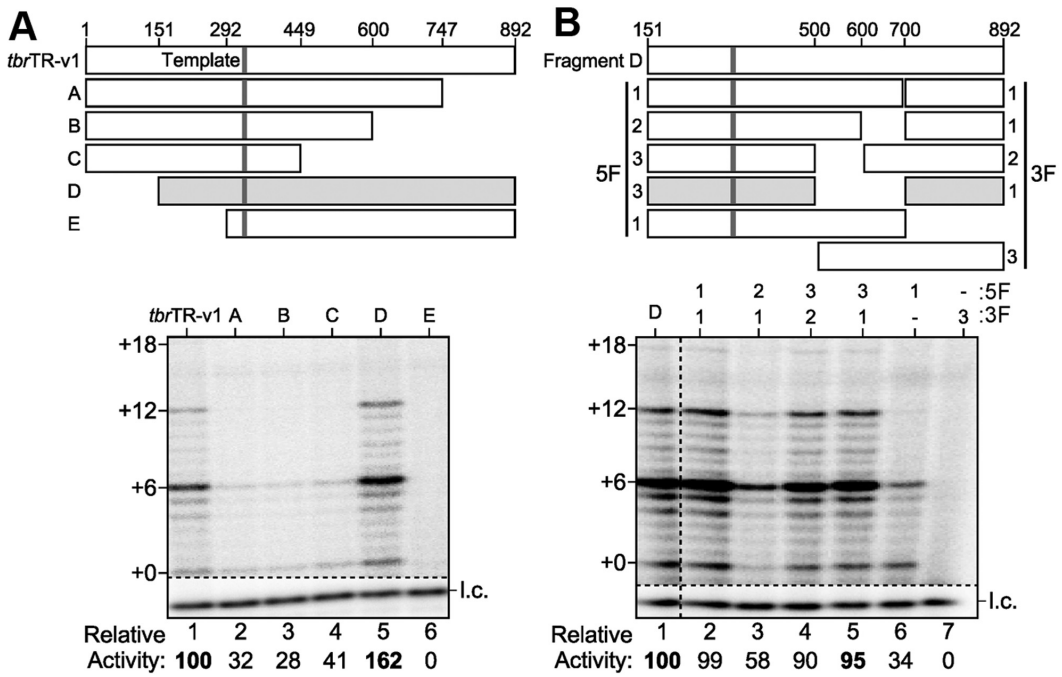

Figure 2. Identification of the minimal *tbr*TR regions for telomerase activity**.** (**A**) Truncation analysis of *tbr*TR. (Top) Schematic of *tbr*TR-v1 with 5′- and 3′- serial truncation fragments A–E. Each RNA fragment retains the 11-nt sequence. The minimal *tbr*TR fragment D that generated the full activity is shaded in grey. (Bottom) Activity assay for *T. brucei* telomerase reconstituted with *tbr*TR 5′- and 3′-truncated fragments. (**B**) Truncation analysis of the *tbr*TR 5′- and 3′-fragments. (Top) Schematic of the truncated *tbr*TR 5′- and 3′-fragments. The *tbr*TR fragment D was divided and truncated to generate the 5F and 3F fragments. (Bottom) Activity assay of telomerase reconstituted from the *tbr*TR 5F and 3F truncated fragments in various combinations. The minimal *tbr*TR fragments that generated the full activity are shaded in grey. A ^{32}P-end-labeled 18-mer DNA primer was added prior to product purification as a loading control (l.c.) for DNA product recovery and loading. The number of nucleotides added to the primer are denoted beside the gel with the relative activity shown below the gel. Numbers above the *tbr*TR and fragment D schematics denote the nucleotide position within the RNA.

erase function. Similar helical truncations were introduced into the base of the 3F1 putative stem-loop to generate the four fragments, 3F1-a to -d (Figure 3C, top). Of the telomerases reconstituted with these 3F1 truncated RNA fragments, together with the 5F3 fragment and *tbr*TERT, fragment 3F1-c that spanned residues 781–819 represented the minimal region as it reconstituted activity similar to the parental 3F1 fragment (Figure 3C, bottom, lane 4). Fragments 3F1-e and -f had residues 795–806 and 786–814, respectively, replaced with a GAAA tetraloop to stabilize the truncated helical structures. These 3F1 fragments produced background telomerase activity similar to the 5F3 fragment alone (Figure 3C, bottom, lanes 6–8). Thus, the majority of the putative 3F1 stem-loop is dispensable, with merely the 39 nt apical stem-loop essential for optimal telomerase activity.

Secondary structure determination of *T. brucei* TR core domains

We then sought to validate and improve the predicted secondary structure of the two minimal *tbr*TR functional domains by chemical probing as well as phylogenetic comparative sequence analysis. For chemical probing, we initially performed selective 2′-hydroxyl acylation analysis by primer extension (SHAPE) assay on *in vitro* T7 transcribed RNA fragments of *tbr*TR to probe for the flexible unpaired regions in the folded RNA. The 202 nt 5F3-g and 46 nt 3F1-b RNA fragments were synthesized with SHAPE adapter stem-loops appending the 5′- and 3′-ends for primer annealing and down-stream analysis (Supplementary Figure S2A and S2C). The synthesized RNA fragments were folded *in vitro* independently, treated with *N*-methylisatoic anhydride (NIMA) that chemically modifies the 2′-hydroxyl of unpaired bases, and analyzed by primer extension to identify the NIMA-modified, unpaired residues in the folded RNA (Figure 4A and B, Supplementary Figure S2B and S2D). These SHAPE chemical probing data were then used to improve the predicted secondary structures of the two minimal *tbr*TR functional domains. The template-harboring *tbr*TR fragment, herein termed the template core domain, comprises three helices, Helix-I, -II and -III (Figure 4C). The template-distal domain is termed the eCR4/5 domain as it is functionally equivalent to the vertebrate and fungal CR4/5 domain (8), yet structurally distinct by comprising a stem-loop with an internal loop separating two base-paired regions, termed Helix-IVa and -IVb (Figure 4C).

Beyond the SHAPE structural probing, we performed phylogenetic comparative co-variation analysis with the sequences of available trypanosome TR homologs (25,26) to lend support for the base-paired helical regions in the folded RNA. In addition to the four recently identified trypanosome TR species, we identified a TR homolog from the draft genome of the African crocodilian trypanosome *T. grayi* (31). *T. grayi* TR was identified using the Fragrep2 program (32) and a position weight matrix derived from the sequence alignment of the four known trypanosome TR

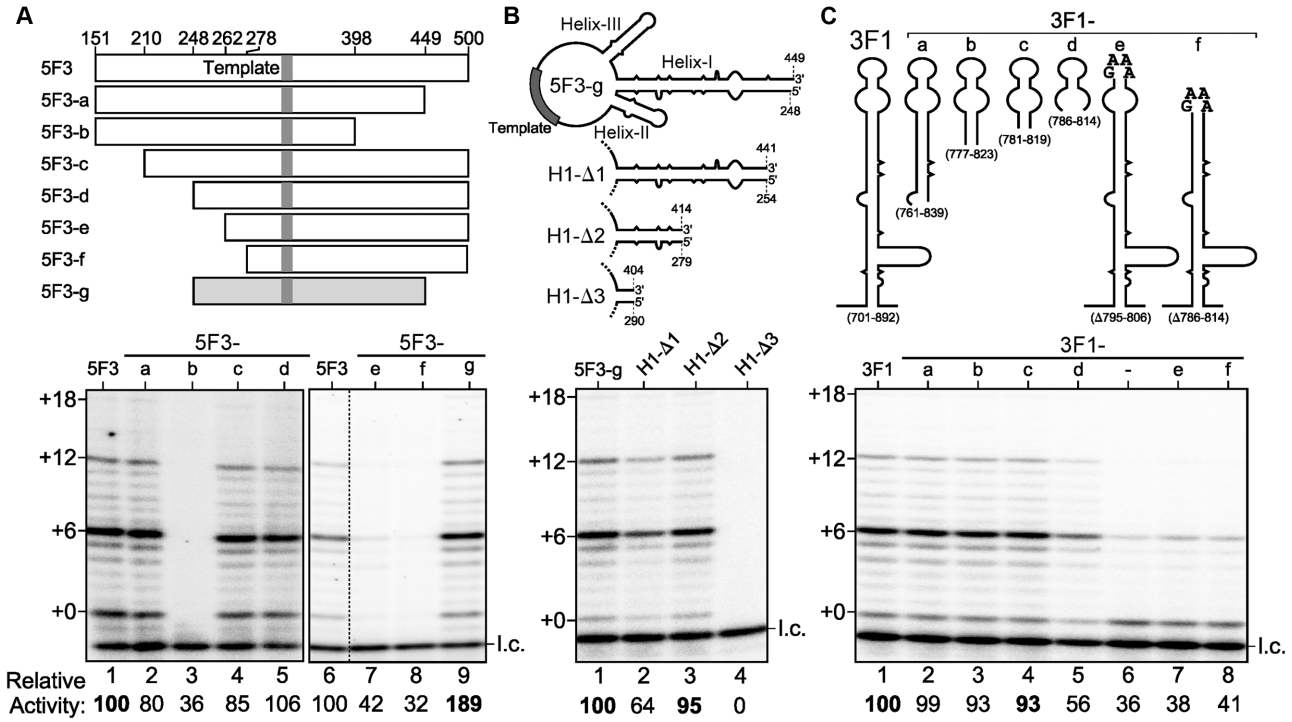

Figure 3. Structure-based truncation analysis of *tbr*TR. (**A**) Truncation analysis of the *tbr*TR 5F3 fragment. (Top) Schematic of the *tbr*TR 5F3 truncated fragments, 5F3-a to -g. The template within each fragment is denoted. The minimal 5F3 fragment required for telomerase activity is shaded in grey. (Bottom) Activity assay of telomerase reconstituted from the truncated *tbr*TR 5F3 fragments. Numbers above the *tbr*TR 5F3 fragment schematic denotes the nucleotide position within the RNA. (**B**–**C**) Structure-based truncation analysis of the *tbr*TR 5′ and 3′ fragments 5F3-g and 3F1. (Top) Outlines of the predicted secondary structures for the *tbr*TR 5Fi and 3F1 fragments. Truncations from the apical loop were capped by the GAAA tetraloop. (Bottom) Activity assay of telomerase reconstituted from *tbr*TR 5F3-g and 3F1 truncated fragments. A ^{32}P-end-labeled 18-mer DNA primer was added prior to product purification as a loading control (l.c.) for DNA product recovery and loading. The number of nucleotides added to the primer are denoted beside the gel with the relative activity shown below the gel.

species (see Materials and Methods). This putative TR from *T. grayi* is seemingly authentic based on the presence and position of the box C and D sequence motifs, the invariant 11-nt template sequence 3′-AUCCCAAUCCC-5′, and comparable overall sequence conservation (Supplementary Figure S3). From the multiple sequence alignment of these five trypanosome TR sequences, we identified nucleotide co-variations that provide strong support for three base-paired regions, Helix-II and -III and -IVa, in the secondary structures of the two *tbr*TR domains (Figure 4C). However, phylogenetic comparative sequence analysis did not reveal any nucleotide co-variations to support Helix-I in the template core domain or Helix-IVb in the eCR4/5 domain, which were supported by the SHAPE data (Figure 4A and B, Supplementary Figure S2B and S2D). The overall architecture of the *tbr*TR template core domain resembles the ciliate TR secondary structure, containing a core-enclosing helix I, a template-adjacent stem-loop helix II and a stem-loop helix III downstream of the template (17) (Figure 4C). The template-distal eCR4/5 domain however, is located at a great distance from the template core domain, resembling more the vertebrate–fungal CR4/5 and echinoderm eCR4/5 domains (8,10). In contrast, the ciliate TR helix IV is located immediately adjacent to helix I in the highly compact TR structure (36).

Functional characterization of *T. brucei* TR core domains

With this secondary structure model, we then proceeded to investigate the specific function for each of these helical regions within the template core and eCR4/5 domains by mutagenesis analysis and functional assay. The functional analysis of *tbr*TR Helix-I indicated that the basal portion of this helix is crucial for *T. brucei* telomerase activity, as any mutations or truncations that disrupted the base-paired region or removed part of Helix-I abolished activity (Supplementary Figure S1). The template-adjacent stem-loop in known TRs functions as a template boundary element to ensure proper DNA synthesis termination at the end of the template (8,10,37–39). To investigate the necessity of *tbr*TR Helix-II in the template core domain for telomerase activity and template boundary definition, we replaced the apical loop and terminal stem-loop of Helix-II with a GAAA tetraloop to generate mutants H2-ΔL and -ΔLAS, respectively (Figure 5A, top). Additionally, we introduced disruptive and compensatory mutations into the apical stem of Helix-II to generate mutants H2-m1, -m2 and -m3, or into the basal stem to generate mutants H2-m4, -m5 and -m6 (Figure 5A, top). The reconstituted telomerase mutants were examined for activity and template boundary bypass due to disruption of the boundary element. Unexpectedly, none of the active Helix-II mutants were defective in template boundary definition, as these mutant enzymes gener-

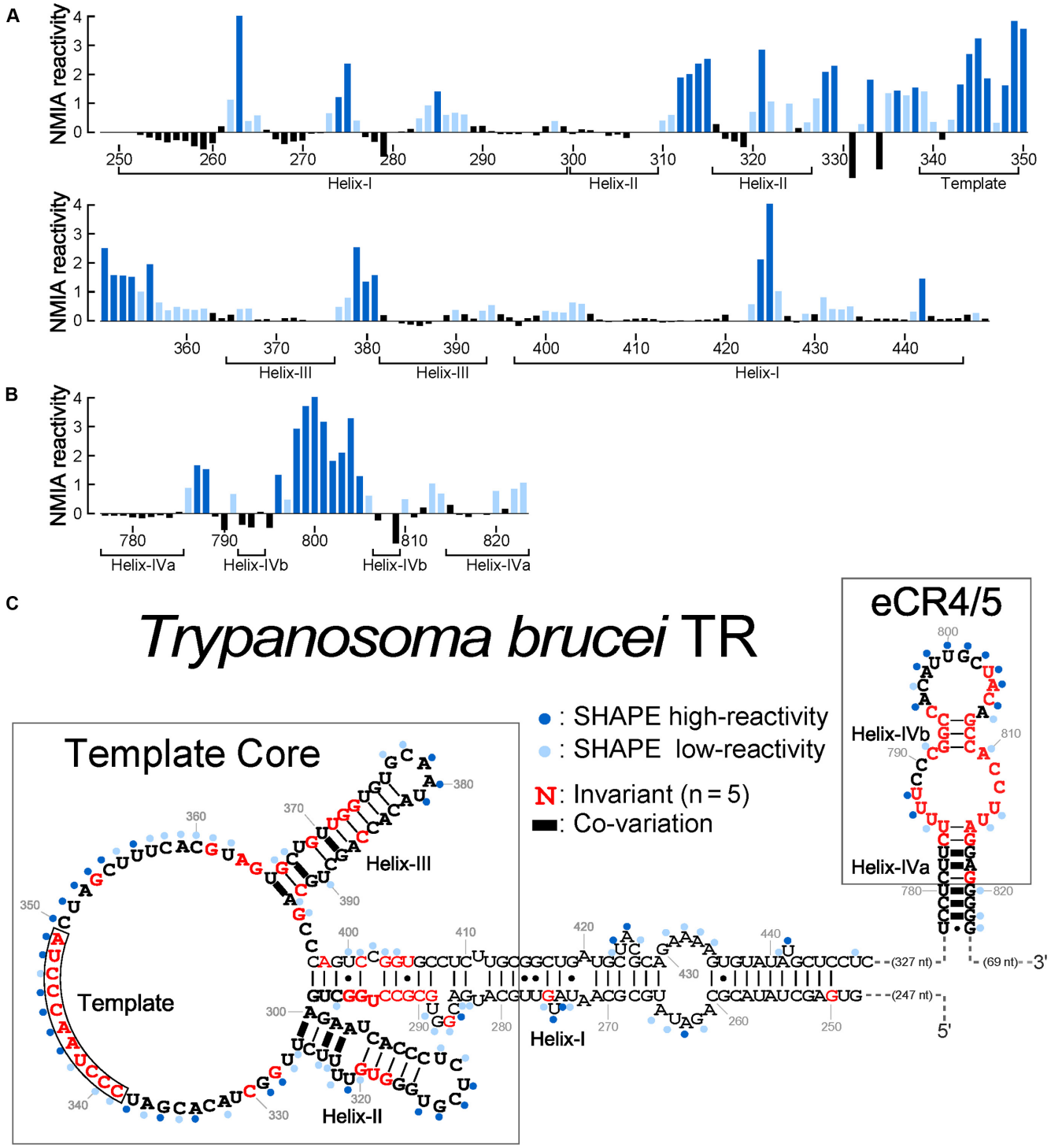

Figure 4. Secondary structure determination of *tbr*TR essential core domains. (**A–B**) SHAPE analysis of *tbr*TR fragments 5F3-g and 3F1-b. Normalized NMIA chemical reactivity was determined by subtracting the intensity values of the DMSO control from the corresponding NMIA reaction (Supplementary Figure S2). The plot denotes high (dark blue), low (light blue) and no (black) NMIA reactivity. Nucleotide position in *tbr*TR-v1 variant and secondary structural features are labeled. (**C**) Secondary structure of *tbr*TR core domains inferred from SHAPE and phylogenetic co-variation analyses. Individual residue flexibility (high, dark blue dots; low, light blue dots) probed by SHAPE analysis are mapped onto the secondary structure. The absolute conservation of specific nucleotides (red) and co-variations (black bars) were derived from the multiple sequence alignment of five trypanosome TRs (Supplementary Figure S3). The nucleotide positions are based on the numbering of the *tbr*TR-v1 variant. The length of the intervening sequences between the functional regions of *tbr*TR is denoted. The region corresponding to the minimal *tbr*TR H1-Δ2 and 3F1-c fragments are termed 'template core' and 'eCR4/5' domains, respectively.

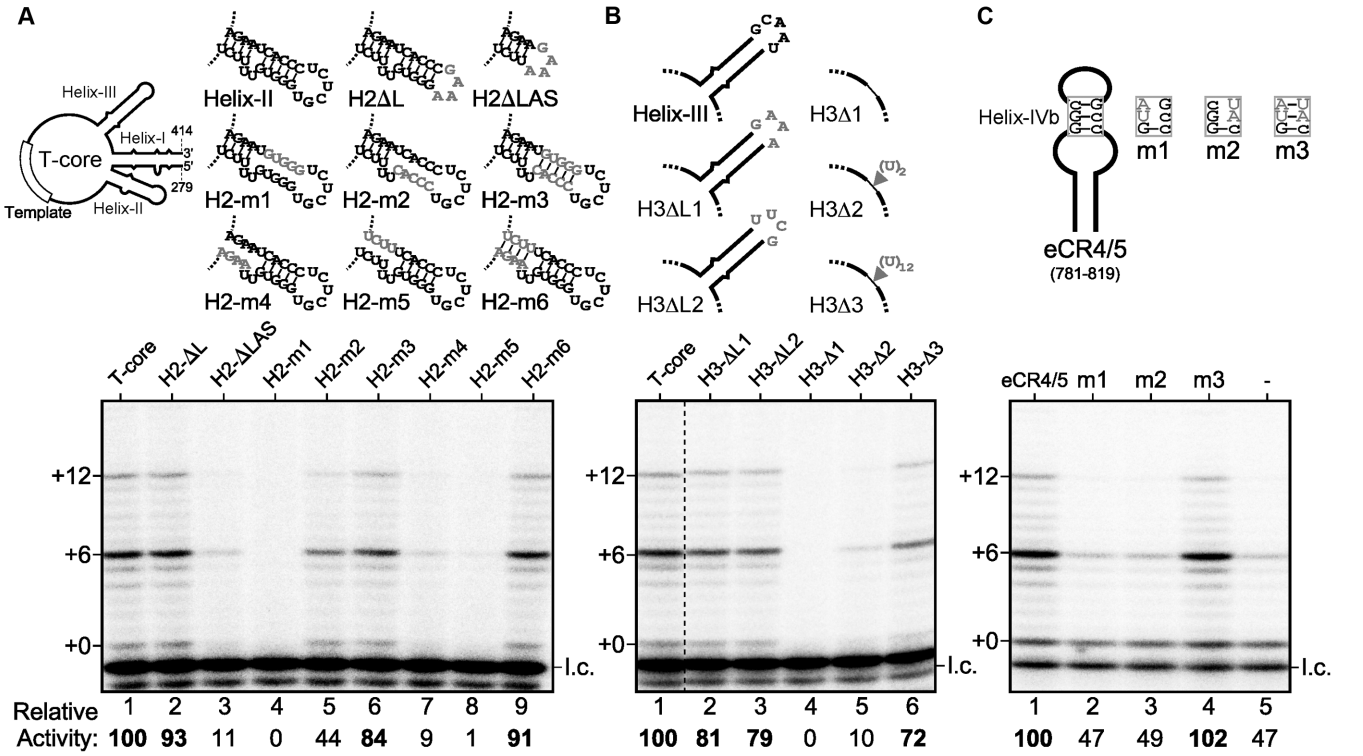

Figure 5. Mutational analysis of the helical regions in the template core and eCR4/5 domains. (**A**) (Top) Truncations of the Helix-II apical loop (H2-ΔL) and apical stem-loop (H2-ΔLAS) were capped by a tetraloop GAAA. Disruptive (-m1, -m2, -m4 and -m5) and compensatory (-m3 and -m6) mutations were introduced to the two base-paired regions of Helix-II. (**B**) (Top) Truncations of the Helix-III apical loop (H3–ΔL1 and –ΔL2) were capped by tetraloops GAAA or UUCG, respectively. Helix-III was removed from the *tbr*TR template core (T-core) fragment to generate H3-Δ1, and replaced with either 2 or 12 rU residues to generate H3-Δ2 and -Δ3, respectively. (**C**) (Top) Disruptive and compensatory mutations introduced into the Helix-IVb. (**A–C**, bottom) Activity assays of *T. brucei* telomerase reconstituted from *tbr*TR fragments with mutations in Helix-II, Helix-III and Helix-IVb. A ^{32}P-end-labeled 18-mer DNA primer was added prior to product purification as a loading control (l.c.) for DNA product recovery and loading. The number of nucleotides added to the primer are denoted beside the gel with the relative activity shown below the gel.

ated the hallmark 6-nt ladder banding pattern of products (Figure 5A, bottom). Interestingly, mutant H2-ΔLAS practically abolished activity (Figure 5A, bottom, lane 3), while mutant H2-ΔL had no significant effect (Figure 5A, bottom, lane 2), indicating that the Helix-II apical loop is dispensable and apical stem is critical for TR function. Mutants H2-m1, -m2, -m4 and -m5 that disrupted base-paired regions of Helix-II severely reduced activity (Figure 5A, lanes 4, 5, 7 and 8), while the compensatory mutants H2-m3 and -m6 restored the base-paired helical structure and effectively rescued activity (Figure 5A, lanes 6 and 9). This suggests that the helical structure and not the specific sequence is critical for telomerase activity. Helix-II would seem to be important for TERT binding, or the overall architecture of the *tbr*TR, and not simply a template boundary element. We then investigated whether the distance between the template and Helix-II is important for template boundary definition. Three cytidine residues were inserted into the linker between the template and Helix-II to generate the Ins-2 mutant. Reconstitution of *T. brucei* telomerase with the Ins-2 mutant resulted in template bypass and usage of the template flanking uridine and adenosine residues as template (Supplementary Figure S4, lanes 1 and 3). Mutant Ins-1 with a similar three cytidine insertion into Helix-I severally damaged reconstituted activity, consistent with the functional importance of Helix-I (Supplementary Figure S4, lane 2). Thus, the template boundary within *tbr*TR is dependent on the length of the linker between the template and Helix-II.

The third stem-loop, Helix-III, within the template core domain appears to be dispensable. Numerous disruptive mutations introduced to Helix-III did not affect the activity of reconstituted telomerase (data not shown). We then investigated whether *T. brucei* telomerase activity would be affected by the elimination of the entire Helix-III from *tbr*TR. The apical loop of Helix-III was replaced by a GAAA or UUCG tetraloop to generate H3-ΔL1 and –ΔL2, respectively (Figure 5B, top). Additionally, Helix-III was completely removed and subsequently replaced by various rU residues to generate mutants H3-Δ1, -Δ2 and -Δ3. The mutants H3-ΔL1 and –ΔL2 that had the Helix-III apical loop removed still reconstituted telomerases with a high level of activity (Figure 5B, lanes 2 and 3). In contrast, the complete removal of Helix-III in the H3-Δ1 mutant completely abolished activity (Figure 5B, lane 4). The insertion of 2 rU residues in the H3-Δ2 mutant slightly rescued activity, while the replacement of Helix-III with 12 rU residues in the H3-Δ3 mutant substantially restored activity (Figure 5B, lane 4–6). Therefore, Helix-III does not seem crucial for *tbr*TR function, yet a minimal number of residues connecting the flanking regions of Helix-III seem necessary.

The template-distal eCR4/5 domain of *tbr*TR forms a unique structural element, functioning for the stimulation of telomerase activity. This esoteric structure harbors a short putative three base-pair stem, Helix-IVb, that is located between the large apical and internal loops (Figure 4C). The absolute conservation of this putative three base-pair helix impedes co-variation sequence analysis (Supplementary Figure S3C). To determine the requirement of this exceedingly short helix for the function of *tbr*TR eCR4/5, we performed disruptive and compensatory mutagenesis of these three base-pairs (Figure 5C, top). Disruption of these base-pairings by mutagenesis of either strand abolished the stimulatory effect of eCR4/5, resulting in telomerase activity similar to the omission of eCR4/5 (Figure 5C, lanes 2, 3 and 5), while the compensatory mutation of both strands restored these base-pairings and rescued the lost activity (Figure 5C, lane 4). Thus, the *tbr*TR eCR4/5 domain relies on its peculiar structure for the stimulation of telomerase activity.

DISCUSSION

Discerning the common ancestral features and the origins of TR has remained a daunting challenge. The scarcity of 'molecular fossils' is further compounded by the rapid evolution and diversification of TRs, complicating the very identification and structure determination of TRs from groups of species outside of vertebrate, yeast and ciliate lineages. Nonetheless, there has been considerable progress in determining the common ancestral TR features for metazoans and fungi following the identification and structure determination of filamentous fungal TRs (8). The vertebrate CR4/5 domain was found to be well-conserved throughout the expansive fungal clade, Pezizomycotina, and even within fission yeast TR. The conservation of CR4/5 within fungal and vertebrate TRs supports a common ancestor with a domain similar to CR4/5 (Figure 6). Moreover, budding yeast TRs with a more degenerate three-way-junction of helices in place of CR4/5 are likely an evolutionary offshoot (15). However, there has remained a large discrepancy and unresolved evolutionary connection amongst the metazoan-fungal lineage—with their large TRs comprising two distinct structural domains that can function *in trans* (8,40,41)—and the highly-compact and diminutive ciliate TRs that function poorly *in trans* compared to a single fragment (42). To resolve the disparity amongst TRs from the ciliated protozoan and metazoan-fungal lineages and discern the features of the common ancestral TR for eukaryotes, we have determined the minimal TR functional domains from the early emerging eukaryote, the flagellated protozoan *T. brucei*.

Flagellate TR comprises two distinct structural domains that are together required for full activity and are located ∼350 nt apart within the RNA (Figure 4C), similar to that of the TRs from the metazoan-fungal lineage (Figure 6). These two structural domains can be excised from the vastly larger, ∼1000 nt, *tbr*TR and are presumably bound by the *tbr*TERT protein *in trans* as separate RNA fragments (Figure 2B). The commonality of these functional features within flagellates, vertebrates and fungi strongly supports the common ancestor for TRs similarly comprised

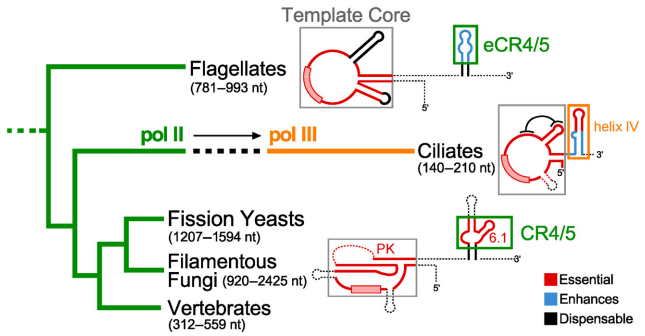

Figure 6. Comparison of TR essential core domains from flagellate, ciliate and metazoan-fungal lineages. (Left) Phylogenetic relationship of representative eukaryotic lineages (28). TR in most species is transcribed by RNA pol II (green) with a specific and unique transition event to RNA pol III (dashed line, arrow) within the ciliate lineage (orange). TR size variation is denoted below each group of species. (Right) Schematic secondary structures of the two TR core domains. Within the two TR core domains, elements that are absolutely required for basal telomerase activity are denoted (red) and generally comprise the template core domain along with the CR4/5 domain for vertebrates, filamentous fungi and fission yeasts (8). Elements that increase telomerase activity above basal activity (blue) and dispensable regions within the TR for activity *in vitro* (black) are denoted. Ciliate TR requires helix IV *in cis* for full activity and the apical stem-loop of helix IV generates only partial activity *in trans* (42). Variable regions are depicted as dashed lines within the structure. The common structure of TR core domains from metazoans, fission yeast and filamentous fungi is depicted.

two structural domains that are separated by a variable distance within the endogenous RNA and can function with the TERT protein either *in cis* as a single RNA transcript or *in trans* as two independent RNA fragments.

A template-proximal pseudoknot structure with a critical triple helix has been a defining feature of TRs. However, the early diverging trypanosome TRs lack apparent pseudoknot structures (Figure 4C) and ciliate TR pseudoknots are weakly-defined structures with few base-pairings, which is functionally dispensable for *in vitro* ciliate telomerase activity (43). This suggests that the TR pseudoknot structure progressively evolved along the metazoan-fungal lineage to become functionally essential for telomerase enzymatic activity (44,45). Extensive phylogenetic comparative sequence analysis in the sequence flanking the *tbr*TR Helix-III—the most likely region for the formation of a similar pseudoknot structure within trypanosome TR—did not reveal convincing nucleotide co-variations to support a pseudoknot structure, as opposed to the higher conservation and co-variations within the simple pseudoknot structures of ciliate TRs (Supplementary Figure S5). Moreover, we found no empirical support for a pseudoknot structure by SHAPE analysis (Figure 4A, Supplementary Figure S2B) and the entire Helix-III is dispensable for the reconstitution of *T. brucei* telomerase activity (Figure 5B). Nonetheless, *T. brucei* Helix-III may potentially form base-triples with the flanking regions in the apparent absence of a pseudoknot structure as TR pseudoknot structures from fungi and vertebrates possess higher-order base-triples that are crucial for telomerase function (44–46) and further tertiary structural analysis would be necessary. These results suggest that the common ancestral TR lacked a complicated pseudo-

knot structure, or even any pseudoknot structure, and later acquired this critical structure and triple helix feature over the course of evolution (Figure 6).

The second critical TR domain for telomerase activity is the template-distal stem-loop moiety, the CR4/5 domain in vertebrates and fungi. The *tbr*TR structure comprises an eCR4/5 domain—functionally equivalent to the vertebrate-fungal CR4/5 domain—which is capable of assembling with *tbr*TERT *in trans* for telomerase enzymatic activity (Figure 6). However, the *tbr*TR eCR4/5 domain contains an important three base-pair helix flanked by large apical and internal loops (Figure 4C), lacking the implied metazoan-fungal common ancestral TR three-way-junction of helices. The omission of the metazoan-fungal P6.1 stem-loop correlates with the reduced requirement of the *tbr*TR eCR4/5 domain for telomerase activity, merely functioning to stimulate activity and is similar to the echinoderm template-distal stem-loop moiety (10). This would strongly suggest that the specific CR4/5 structure, with the absolutely essential P6.1 stem-loop, likely emerged along the metazoan–fungal lineage (Figure 6).

The ancestry of two distinct structural domains located at a distance within the RNA suggests that ciliate TRs are divergent with more unique and non-conserved features. Ciliate TR helix IV reconstitutes limited telomerase activity *in trans* (42) and is possibly a functional analog of the eCR4/5 and CR4/5 domains. This reduced functionality of ciliate helix-IV is presumably from weaker TERT protein affinity (42), a potential consequence of the compact size of ciliate TR—at only 140–210 nt in length—and the close proximity of helix IV to the template core domain. The proper positioning of the ciliate Helix-IV apical loop in the telomerase RNP complex requires ciliate-specific helical bending induced by p65 protein binding (36,47). The dramatic diminution of ciliate TRs is likely a repercussion of the evolutionary transition for TR synthesis from RNA pol II to pol III. RNA pol III transcribes specifically small RNAs and terminates transcription at poly(U) tracts that would have truncated an ancestral and presumably larger ciliate TR gene at U-rich sites. It is highly conceivable that an ancestral CR4/5 or eCR4/5 element would lie downstream of a U-rich site and therefore would have been lost in the RNA pol II to pol III transition event.

The *tbr*TR template core domain alone generates a basal level of telomerase activity (Figure 2B, lane 6). The ancestral ciliate TR template core domain presumably also retained a basal level of activity that would have facilitated the convergent evolution of ciliate Helix IV as a *de novo* analog emerged to substitute for the lost CR4/5 or eCR4/5 domain. In addition to flagellate TR, echinoderm TRs also generate significant telomerase activity without their respective template-distal eCR4/5 domains (10). However, ciliate telomerase is highly dependent on the presence of helix IV, the loss of helix IV virtually abolishes enzymatic activity (42). While potentially possible—yet seemingly implausible, ciliate TR may have sufficiently contracted in size and lacked internal U-rich tracts before the transition to RNA pol III to retain its ancestral eCR4/5 element. This would suggest that ciliate helix IV is a highly degenerate CR4/5 or eCR4/5 element that lost independent binding functionality. Regardless of the transition pathway to RNA pol III, ciliate TRs appears to be evolutionary outliers.

Determining the minimal flagellate TR structural domains has resolved the sharp divide amongst the implied metazoan–fungal common ancestor and the divergent ciliate TRs. The functional conservation of two distinct structural domains in flagellate TR brings a glimpse of the ancient progenitor TR and the emergence of the ubiquitous telomerase enzyme. The common ancestor for TR would have emerged with two TERT binding domains, comprising a template core and distal stem-loop moiety. The template core domain putatively functions for positioning the template within proximity to the TERT active site and the template-distal stem-loop moiety possibly functions to reinforce the TERT active site itself, demonstrating the interdependence between TR and TERT for telomerase RNP assembly and enzymatic function.

SUPPLEMENTARY DATA

Supplementary Data are available at NAR Online.

ACKNOWLEDGEMENT

The authors are grateful to Dr. Juan Alfonzo for providing *T. brucei* genomic DNA.

FUNDING

National Institutes of Health (NIH) [GM094450 to J.J.-L.C.]. Funding for open access charge: National Institutes of Health (NIH) [GM094450 to J.J.-L.C.].
Conflict of interest statement. None declared.

REFERENCES

1. de Lange,T. (2015) A loopy view of telomere evolution. *Front. Genet.*, **6**, 321.
2. Price,C.M., Boltz,K.A., Chaiken,M.F., Stewart,J.A., Beilstein,M.A. and Shippen,D.E. (2010) Evolution of CST function in telomere maintenance. *Cell Cycle*, **9**, 3157–3165.
3. Blackburn,E.H., Epel,E.S. and Lin,J. (2015) Human telomere biology: A contributory and interactive factor in aging, disease risks, and protection. *Science*, **350**, 1193–1198.
4. de Lange,T. (2004) T-loops and the origin of telomeres. *Nat. Rev. Mol. Cell Biol.*, **5**, 323–329.
5. Podlevsky,J.D. and Chen,J.J.-L. (2012) It all comes together at the ends: telomerase structure, function, and biogenesis. *Mutat. Res.*, **730**, 3–11.
6. Podlevsky,J.D., Bley,C.J., Omana,R.V., Qi,X. and Chen,J.J.-L. (2008) The telomerase database. *Nucleic Acids Res.*, **36**, D339–D343.
7. Lin,J., Ly,H., Hussain,A., Abraham,M., Pearl,S., Tzfati,Y., Parslow,T.G. and Blackburn,E.H. (2004) A universal telomerase RNA core structure includes structured motifs required for binding the telomerase reverse transcriptase protein. *Proc. Natl Acad. Sci. U.S.A.*, **101**, 14713–14718.
8. Qi,X., Li,Y., Honda,S., Hoffmann,S., Marz,M., Mosig,A., Podlevsky,J.D., Stadler,P.F., Selker,E.U. and Chen,J.J.-L. (2013) The common ancestral core of vertebrate and fungal telomerase RNAs. *Nucleic Acids Res.*, **41**, 450–462.
9. Blackburn,E.H. and Collins,K. (2011) Telomerase: an RNP enzyme synthesizes DNA. *Cold Spring Harb. Perspect. Biol.*, **3**, 1–9.
10. Podlevsky,J.D., Li,Y. and Chen,J.J.-L. (2016) Structure and function of echinoderm telomerase RNA. *RNA*, **22**, 204–215.
11. Zhang,Q., Kim,N.-K. and Feigon,J. (2011) Architecture of human telomerase RNA. *Proc. Natl Acad. Sci. U.S.A.*, **108**, 20325–20332.

12. Chen,J.-L., Opperman,K.K. and Greider,C.W. (2002) A critical stem-loop structure in the CR4-CR5 domain of mammalian telomerase RNA. *Nucleic Acids Res.*, **30**, 592–597.
13. Bley,C.J., Qi,X., Rand,D.P., Borges,C.R., Nelson,R.W. and Chen,J.J.-L. (2011) RNA-protein binding interface in the telomerase ribonucleoprotein. *Proc. Natl Acad. Sci. U.S.A.*, **108**, 20333–20338.
14. Huang,J., Brown,A.F., Wu,J., Xue,J., Bley,C.J., Rand,D.P., Wu,L., Zhang,R., Chen,J.J.-L. and Lei,M. (2014) Structural basis for protein-RNA recognition in telomerase. *Nat. Struct. Mol. Biol.*, **21**, 507–512.
15. Brown,Y., Abraham,M., Pearl,S., Kabaha,M.M., Elboher,E. and Tzfati,Y. (2007) A critical three-way junction is conserved in budding yeast and vertebrate telomerase RNAs. *Nucleic Acids Res.*, **35**, 6280–6289.
16. Greider,C.W. and Blackburn,E.H. (1987) The telomere terminal transferase of Tetrahymena is a ribonucleoprotein enzyme with two kinds of primer specificity. *Cell*, **51**, 887–898.
17. McCormick-Graham,M. and Romero,D.P. (1995) Ciliate telomerase RNA structural features. *Nucleic Acids Res.*, **23**, 1091–1097.
18. Qi,X., Rand,D.P., Podlevsky,J.D., Li,Y., Mosig,A., Stadler,P.F. and Chen,J.J.-L. (2015) Prevalent and distinct spliceosomal 3′-end processing mechanisms for fungal telomerase RNA. *Nat. Commun.*, **6**, 6105.
19. Box,J.A., Bunch,J.T., Tang,W. and Baumann,P. (2008) Spliceosomal cleavage generates the 3′ end of telomerase RNA. *Nature*, **456**, 910–914.
20. Kannan,R., Helston,R.M., Dannebaum,R.O. and Baumann,P. (2015) Diverse mechanisms for spliceosome-mediated 3′ end processing of telomerase RNA. *Nat. Commun.*, **6**, 6104.
21. Nguyen,D., Grenier St-Sauveur,V., Bergeron,D., Dupuis-Sandoval,F., Scott,M.S. and Bachand,F. (2015) A polyadenylation-dependent 3′ end maturation pathway is required for the synthesis of the human telomerase RNA. *Cell Rep.*, **13**, 2244–2257.
22. Tseng,C.-K., Wang,H.-F., Burns,A.M., Schroeder,M.R., Gaspari,M. and Baumann,P. (2015) Human telomerase RNA processing and quality control. *Cell Rep.*, **13**, 2232–2243.
23. Gunisova,S., Elboher,E., Nosek,J., Gorkovoy,V., Brown,Y., Lucier,J.-F., Laterreur,N., Wellinger,R.J., Tzfati,Y. and Tomaska,L. (2009) Identification and comparative analysis of telomerase RNAs from Candida species reveal conservation of functional elements. *RNA*, **15**, 546–559.
24. Noël,J.-F., Larose,S., Abou Elela,S. and Wellinger,R.J. (2012) Budding yeast telomerase RNA transcription termination is dictated by the Nrd1/Nab3 non-coding RNA termination pathway. *Nucleic Acids Res.*, **40**, 5625–5636.
25. Sandhu,R., Sanford,S., Basu,S., Park,M., Pandya,U.M., Li,B. and Chakrabarti,K. (2013) A trans-spliced telomerase RNA dictates telomere synthesis in Trypanosoma brucei. *Cell Res.*, **23**, 537–551.
26. Gupta,S.K., Kolet,L., Doniger,T., Biswas,V.K., Unger,R., Tzfati,Y. and Michaeli,S. (2013) The Trypanosoma brucei telomerase RNA (TER) homologue binds core proteins of the C/D snoRNA family. *FEBS Lett.*, **587**, 1399–1404.
27. Lukes,J., Hashimi,H. and Zíková,A. (2005) Unexplained complexity of the mitochondrial genome and transcriptome in kinetoplastid flagellates. *Curr. Genet.*, **48**, 277–299.
28. Cavalier-Smith,T., Chao,E.E., Snell,E.A., Berney,C., Fiore-Donno,A.M. and Lewis,R. (2014) Multigene eukaryote phylogeny reveals the likely protozoan ancestors of opisthokonts (animals, fungi, choanozoans) and Amoebozoa. *Mol. Phylogenet. Evol.*, **81**, 71–85.
29. Cohen,S.B. and Reddel,R.R. (2008) A sensitive direct human telomerase activity assay. *Nat. Methods*, **5**, 355–360.
30. Wilkinson,K.A., Merino,E.J. and Weeks,K.M. (2006) Selective 2′-hydroxyl acylation analyzed by primer extension (SHAPE): quantitative RNA structure analysis at single nucleotide resolution. *Nat. Protoc.*, **1**, 1610–1616.
31. Kelly,S., Ivens,A., Manna,P.T., Gibson,W. and Field,M.C. (2014) A draft genome for the African crocodilian trypanosome Trypanosoma grayi. *Sci. Data*, **1**, 140024.
32. Mosig,A., Sameith,K. and Stadler,P. (2006) Fragrep: an efficient search tool for fragmented patterns in genomic sequences. *Genomics Proteomics Bioinformatics*, **4**, 56–60.
33. Collins,K. and Greider,C.W. (1993) Tetrahymena telomerase catalyzes nucleolytic cleavage and nonprocessive elongation. *Genes Dev.*, **7**, 1364–1376.
34. Huard,S. and Autexier,C. (2004) Human telomerase catalyzes nucleolytic primer cleavage. *Nucleic Acids Res.*, **32**, 2171–2180.
35. Zuker,M. (2003) Mfold web server for nucleic acid folding and hybridization prediction. *Nucleic Acids Res.*, **31**, 3406–3415.
36. Jiang,J., Chan,H., Cash,D.D., Miracco,E.J., Ogorzalek Loo,R.R., Upton,H.E., Cascio,D., O'Brien Johnson,R., Collins,K., Loo,J.A. *et al.* (2015) Structure of Tetrahymena telomerase reveals previously unknown subunits, functions, and interactions. *Science*, **350**, aab4070.
37. Lai,C.K., Miller,M.C. and Collins,K. (2002) Template boundary definition in Tetrahymena telomerase. *Genes Dev.*, **16**, 415–420.
38. Box,J.A., Bunch,J.T., Zappulla,D.C., Glynn,E.F. and Baumann,P. (2008) A flexible template boundary element in the RNA subunit of fission yeast telomerase. *J. Biol. Chem.*, **283**, 24224–24233.
39. Chen,J.-L. and Greider,C.W. (2003) Template boundary definition in mammalian telomerase. *Genes Dev.*, **17**, 2747–2752.
40. Tesmer,V.M., Ford,L.P., Holt,S.E., Frank,B.C., Yi,X., Aisner,D.L., Ouellette,M., Shay,J.W. and Wright,W.E. (1999) Two inactive fragments of the integral RNA cooperate to assemble active telomerase with the human protein catalytic subunit (hTERT) in vitro. *Mol. Cell. Biol.*, **19**, 6207–6216.
41. Mitchell,J.R. and Collins,K.L. (2000) Human telomerase activation requires two independent interactions between telomerase RNA and telomerase reverse transcriptase. *Mol. Cell*, **6**, 361–371.
42. Mason,D.X., Goneska,E. and Greider,C.W. (2003) Stem-loop IV of tetrahymena telomerase RNA stimulates processivity in trans. *Mol. Cell. Biol.*, **23**, 5606–5613.
43. Autexier,C. and Greider,C.W. (1998) Mutational analysis of the Tetrahymena telomerase RNA: identification of residues affecting telomerase activity in vitro. *Nucleic Acids Res.*, **26**, 787–795.
44. Shefer,K., Brown,Y., Gorkovoy,V., Nussbaum,T., Ulyanov,N.B. and Tzfati,Y. (2007) A triple helix within a pseudoknot is a conserved and essential element of telomerase RNA. *Mol. Cell. Biol.*, **27**, 2130–2143.
45. Theimer,C.A., Blois,C.A. and Feigon,J. (2005) Structure of the human telomerase RNA pseudoknot reveals conserved tertiary interactions essential for function. *Mol. Cell*, **17**, 671–682.
46. Cash,D.D., Cohen-Zontag,O., Kim,N.-K., Shefer,K., Brown,Y., Ulyanov,N.B., Tzfati,Y. and Feigon,J. (2013) Pyrimidine motif triple helix in the Kluyveromyces lactis telomerase RNA pseudoknot is essential for function in vivo. *Proc. Natl Acad. Sci. U.S.A.*, **110**, 10970–10975.
47. Stone,M.D., Mihalusova,M., O'Connor,C.M., Prathapam,R., Collins,K. and Zhuang,X. (2007) Stepwise protein-mediated RNA folding directs assembly of telomerase ribonucleoprotein. *Nature*, **446**, 458–461.